Cytosolic nucleotides block and regulate the Arabidopsis vacuolar anion channel AtALMT9

Zhang, Jingbo ; Martinoia, Enrico ; De Angeli, Alexis

Abstract: The aluminum-activated malate transporters (ALMTs) form a membrane protein family exhibiting different physiological roles in plants, varying from conferring tolerance to environmental Al(3+) to the regulation of stomatal movement. The regulation of the anion channels of the ALMT family is largely unknown. Identifying intracellular modulators of the activity of anion channels is fundamental to understanding their physiological functions. In this study we investigated the role of cytosolic nucleotides in regulating the activity of the vacuolar anion channel AtALMT9. We found that cytosolic nucleotides modulate the transport activity of AtALMT9. This modulation was based on a direct block of the pore of the channel at negative membrane potentials (open channel block) by the nucleotide and not by a phosphorylation mechanism. The block by nucleotides of AtALMT9-mediated currents was voltage dependent. The blocking efficiency of intracellular nucleotides increased with the number of phosphate groups and ATP was the most effective cellular blocker. Interestingly, the ATP block induced a marked modification of the current-voltage characteristic of AtALMT9. In addition, increased concentrations of vacuolar anions were able to shift the ATP block threshold to a more negative membrane potential. The block of AtALMT9-mediated anion currents by ATP at negative membrane potentials acts as a gate of the channel and vacuolar anion tune this gating mechanism. Our results suggest that anion transport across the vacuolar membrane in plant cells is controlled by cytosolic nucleotides and the energetic status of the cell.

DOI: https://doi.org/10.1074/jbc.M114.576108

Cytosolic Nucleotides Block and Regulate the *Arabidopsis* Vacuolar Anion Channel *At*ALMT9

Jingbo Zhang[1], Enrico Martinoia[1] and Alexis De Angeli[1,2]

[1]Institute of Plant Biology, University of Zurich, CH-8008 Zurich, Switzerland

[2] Institut des Sciences du Végétal, CNRS, Gif-sur-Yvette, France.

* Running title*: Regulation of an intracellular anion channel by nucleotides*

To whom the correspondence should be addressed: Alexis De Angeli, Institut des Sciences du Végétal CNRS, 1 Avenue de la Terrasse 91198 Gif-sur-Yvette Cedex, France, Tel: +33(0)169823675, Fax: +33(0)169823695. E-mail: alexis.de-angeli@isv.cnrs-gif.fr. Enrico Martinoia, Instute of Plant Biology University of Zurich, Zollikerstrasse 107, 8008 Zurich, Switzerland, Tel: +41 44 63 48222, Fax: 41 44 63 48204, E-mail: enrico.martinoia@botinst.uzh.ch

Keywords: Chloride channels, Membrane transport, Electrophysiology, ATP, Membrane biophysics, open channel blocker, malate, intracellular

Background: AtALMT9 is an intracellular anion channel regulating stomata aperture.

Results: ATP interacts with the pore of AtALMT9 competing with vacuolar anions and modifying the voltage dependency of this ion channel.

Conclusion: cytosolic nucleotides and vacuolar anions directly modulate the transport activity of AtALMT9

Significance: regulation of intracellular transporters is crucial for their physiological functions.

ABSTRACT

The ALuminum Activated Malate Transporters (ALMTs) form a membrane protein family exhibiting different physiological roles in plants, varying from conferring tolerance to environmental Al^{3+} to the regulation of stomatal movement. The regulation of the anion channels of the ALMT family is largely unknown. Identifying intracellular modulators of the activity of anion channels is fundamental to understand their physiological functions. In this study we investigated the role of cytosolic nucleotides in regulating the activity of the vacuolar anion channel *At*ALMT9. We found that cytosolic nucleotides modulate the transport activity of AtALMT9. This modulation was based on a direct block of the channel's pore at negative membrane potentials (open channel block) by the nucleotide and not by a phosphorylation mechanism. The block by nucleotides of AtALMT9 mediated currents was voltage depend. The blocking efficiency of intracellular nucleotides increased with the number of phosphate groups and ATP was the most effective cellular blocker. Interestingly, the ATP block induced a marked modification of the current-voltage characteristic of AtALMT9. In addition, increased concentrations of vacuolar anions were able to shift the ATP block threshold to more negative membrane potential. The block of *At*ALMT9 mediated anion currents by ATP at negative membrane potentials acts as a gate of the channel and vacuolar anion tune this gating mechanism.. Our results suggest that anion transport across the vacuolar membrane in plant cells is controlled by cytosolic nucleotides and the energetic status of the cell.

INTRODUCTION

ALMTs form a membrane protein family exclusive to plants. These proteins have been found to play different important physiological roles. In roots ALMTs are involved in conferring tolerance to environmental Al^{3+} by extruding organic acids in the soil (1-3). In guard-cells they mediate anion fluxes through the plasma and vacuolar membranes and are involved in the regulation of stomatal movements (3-6). The first ALMT channel described, *Ta*ALMT1, was identified as a gene associated to aluminum resistance (2). *Ta*ALMT1 and its homologue in *Arabidopsis thaliana*, *At*ALMT1, catalyse the exudation of malate across the plasma membrane of root cells, resulting in a complexation of Al^{3+} (2,3). Another identified plasma membrane targeted ALMT in *Arabidopsis thaliana* is *At*ALMT12 (5). AtALMT12 is a component of the R-type/QUAC channel of guard cells that mediate the efflux of anions to induce stomata closure (5). *At*ALMT9 was the first vacuolar ALMT identified and characterized in *Arabidopsis thaliana* (4). It was shown that *At*ALMT9 is able to mediate malate and fumarate currents into the vacuole of *Arabidopsis* mesophyll cells. Recently, *At*ALMT9 was shown to play a crucial role in guard cells where it functions as a malate-activated chloride channel involved in stomata opening (6). Moreover, AtALMT9 served as a model to investigate the structural organization of *At*ALMTs . It was reported that *At*ALMT9 assembles as a multimer/tetramers and a region involved in forming the permeation pathway identified (7).

The aim of the present study was to address the question, why the different members of the ALMT family exhibit such striking differences in the current voltage relationships (i.e. I-V curve). The current voltage relationship is a fundamental biophysical characteristic of ion transporters

providing information on their physiological properties. *At*ALMT12, which constitutes part of the R-type/QUAC currents in the plasma membrane of guard cells, exhibits a characteristic "bell-shaped" I-V curve (5,8). The bell-shape of the I-V curve results from an abrupt change in the channel conductance from positive to negative at very negative membrane potentials. This indicates that the channels start to close and the resulting ion current decrease after a critical membrane potential (5,8). In contrast, the other ALMTs exhibit a monotonic voltage dependent I-V curve. This fact indicates that the channels stay open at negative membrane potentials (2-4,6,9). The difference between the I-V characteristics of the ALMTs opens the question of the origin of such a difference. The R-type/QUAC channel of *Arabidopsis* hypocotyl and guard cells was shown to be regulated by cytosolic nucleotides (10-13). In hypocotyl protoplasts it was proposed that cytosolic nucleotides are blockers acting as a "voltage dependent gate" of the R-type/QUAC/*At*ALMT12 channel (13), a gating mode similar to what has been observed in mammalian KIR (potassium inward rectifier) with Mg^{2+} and polyamines (14,15). Surprisingly, after the discovery that ALMTs are part of the R-type/QUAC current the effect of intracellular nucleotides on ALMTs has never been investigated.

In the present study we addressed the question of the origin of the different behavior of the I-V curves of the ALMTs. We used the vacuolar anion channel *At*ALMT9 as a model for ALMT channels with a monotonic I-V curve and found that the cytosolic nucleotides block and regulate *At*ALMT9. The block of *At*ALMT9 by cytosolic nucleotides is voltage dependent and in presence of cytosolic nucleotides the I-V curves becomes bell-shaped similarly to the one of the R-type/QUAC channel. Moreover, the block by cytosolic nucleotides is modulated by the concentration and the nature of the permeable anion present at the cytosolic and the vacuolar side of the channel. The anions at the vacuolar side affect the block by cytosolic nucleotides indicating that the cytosolic nucleotides and the vacuolar anions interact within the permeation pathway of *At*ALMT9. Our data provide a new insight in the regulation of anion channels in the vacuolar membrane.

EXPERIEMNTAL PROCEDURES

Overexpression of AtALMT9-GFP in Nicotiana benthamiana

Agrobacterium tumefaciens (GV3101) was transformed with plasmids containing the sequences of the $AtALMT9_{WT}$ channel and its point mutated derivative $AtALMT9_{K193E}$ by electroporation. The Agrobacterium-mediated infiltration of four week old *Nicotiana benthamiana* leaves was performed as described previously with slight modifications (16). After transient transformation tobacco plants were grown in the greenhouse (16 h light/8 h dark, 25 °C/23 °C, 100 to 200 µmol photons m^{-2} s^{-1}, 60 % relative humidity) for another 2-3 days and then used to isolate protoplasts for patch-clamp experiments.

Electrophysiology

Mesophyll protoplasts from *At*ALMT9-GFP overexpressing tobacco leaves were isolated by enzymatic digestion. The enzyme solution contained 0.3 % (w/v) cellulase R-10, 0.03 % (w/v) pectolyase Y-23, 1 mM $CaCl_2$, 500 mM sorbitol and 10 mM MES, pH 5.3, 550 mOsm. Protoplasts were washed twice and resuspended in the same solution without enzymes. Vacuoles were released from mesophyll protoplasts by the addition of 5 mM EDTA and a slight osmotic shock (500 mOsm, see medium below). Transformed vacuoles exhibiting an *At*ALMT9-GFP signal were selected using an epifluorescence microscope. Membrane currents from tonoplast patches were recorded in the excised cytosolic-side out configuration with the patch-clamp technique as described elsewhere (6,7).

The cytosolic solution contained (i) 100 mM malic acid, adjusted to pH 7.5 with BTP (Bis-Tris-Propane), ii) 30, 50, 100 mM malic acid, supplemented with nucleotides as indicated, adjusted to pH 7.5 with BTP and iii) 100 mM Cl^-, supplemented with nucleotides as indicated, adjusted to pH 7.5 with BTP. The osmolarity was adjusted to 500 mOsm using sorbitol. The pipette

solution contained i) 112 mM malic acid, 5 mM HCl and was adjusted with BTP to pH 6. ii) 10 mM malic acid, 90 mM MES, 5 mM HCl and was adjusted with BTP. iiI) 1 mM malic acid, 99 mM MES, 5 mM HCl and was adjusted with BTP. iv) 100 mM HCl and was adjusted with BTP to pH 6. The osmolarity was adjusted to 550 mOsm using sorbitol. The ionic condition of (i) of cytosolic solution and (i) of the pipette solution is defined as control solution (ctrl). All chemicals were purchased from Sigma-Aldrich. Liquid junction potentials were measured according to Neher (1992) (17) and corrected when higher than ±2 mV.

The dose-response for the ATP_{free} inhibition of $AtALMT9_{WT}$ currents were fitted and analysed with the Langmuir isotherm in the following form:

$$\frac{I}{I_0} = 1 - \frac{1}{1+\frac{K_d^{ATP}}{[ATP]_{cyt}}} \quad (1)$$

where I is the AtALMT9 current amplitude in presence of ATP_{free}, I_0 the AtALMT9 current under control solution, $[ATP]_{cyt}$ the cytosolic ATP concentration, and K_d^{ATP} the dissociation constant of ATP_{free}.

To estimate the fraction of the electrical field that ATP traverses to reach its binding site in Fig. 1B, the voltage-dependent dissociation constant relationship was fitted with the equation described by Woodhull (1973) (18):

$$K_d^{ATP}(V_m) = K_d^{ATP}(0) \cdot e^{\frac{z\delta FV}{RT}} \quad (2)$$

in which $K_d^{ATP}(V_m)$ is the voltage-dependent dissociation constant of ATP, $K_d^{ATP}(0)$ the dissociation constant of ATP at 0 mV, V_m the transmembrane potential, z the valence of the blocker (-4 for ATP at pH=7.5), δ the fraction of the electrical membrane field traversed by the blocker, and F, R, and T the Faraday constant, gas constant and absolute temperature, respectively.

The fraction of currents not blocked by ATP in Fig. 1B, Fig. 2B, Fig. 3B and Fig. 4B were fitted by a Boltzmann function with an offset:

$$\frac{I}{I_0} = I_{unh} + \frac{100 - I_{unh}}{1+e^{\frac{kF(V_{1/2}-V_m)}{RT}}} \quad (3)$$

Where I is the current amplitude in the presence of ATP, I_0 is the current amplitude in a solution without ATP, I_{unh} is the minimum fraction of unblocked current by ATP, $V_{1/2}$ is the potential at which current is half blocked, Vm is the membrane potential, k is a slope factor, F, R, and T the Faraday constant, gas constant and absolute temperature, respectively. Experiments were performed at room temperature (22-25 °C).

Nucleotides

Adenosine-5'-triphosphate (ATP) was tested either as a Mg^{2+} chelate or as a Tris salt (free ATP as indicated). The Adenosine-5'-phosphate (AMP) and Adenosine-5'-diphosphate (ADP) were tested as sodium salt. 5'-adenylylimidodiphosphate (AMPPNP) was Li^{3+} salt. Guanosine-5'-triphosphate (GTP) was Tris salt. All nucleotides were purchased from Sigma-Aldrich.

RESULTS

Cytosolic Nucleotides Inhibit *At*ALMT9 Mediated Currents

In order to test the effect of cytosolic nucleotides on *At*ALMT9-mediated currents we performed patch-clamp experiments in excised cytosolic-side-out configuration using vacuoles extracted from *Nicotiana bentamiana* protoplasts that transiently over-expressed *At*ALMT9-GFP. Under control conditions (30 mM $malate_{cyt}$ / 100 mM $malate_{vac}$), voltage pulses starting from a holding potential of +60 mV ranging to -160 mV in -20 mV steps induced the activation of time-dependent inward malate currents (Fig 1A; (4,6,7)). When 1 mM ATP_{free} was applied at the cytosolic side of the vacuolar membrane (30 mM $malate_{cyt}$ + 1 mM ATP_{cyt} / 100 mM $malate_{vac}$) *At*ALMT9-mediated currents were reversibly inhibited (Fig. 1B,), and similar results were obtained when 1 mM Mg-ATP was applied (Fig. 1G). The presence of 1 mM ATP_{free} in the cytosolic buffer changed the I-V characteristic of *At*ALMT9 from monotonic in control conditions to non-monotonic (i.e. bell-shaped) (Fig 1B, *lower panel*). Notably, the inhibitory effect of ATP_{free} was significantly higher compared to Mg-ATP (Fig. 1H). This indicates that the inhibition is mainly or even exclusively due to ATP_{free} and not to MgATP, the form used in energization

processes. The inhibition by ATP is strongly voltage dependent, being more pronounced at more negative membrane potentials (Fig. 1 B). At -160 mV, the maximum membrane potential we could apply, the currents in the presence of 1 mM ATP_{free} were reduced to 10.5 ± 1.2% of the control currents (30 mM $malate_{cyt}$ + 1 mM ATP_{cyt} / 100 mM $malate_{vac}$; Fig. 1D). The voltage dependency of the inhibition could be adequately described by a Boltzmann function (Eq. 3 in Materials and Method) with an "offset" indicating that at a given ATP_{free} concentration the inhibition never reached 100% at any applied membrane potential (Fig. 1D). We found that the dissociation constant for ATP (K_d^{ATP}) is a function of the membrane potential with K_d^{ATP} = 90 ± 5 µM at -160 mV (Fig. 1E, F). Using the Woodhull formalism (18) to analyze the voltage dependency of K_d^{ATP} we could estimate that ATP transverse ≈ 50% of the applied membrane potential (Fig. 1F,).

The block of *At*ALMT9-mediated currents by ATP was influenced by the cytosolic concentration of the conductive anion (i.e. malate). Cytosolic ATP inhibited *At*ALMT9 currents more at lower cytosolic malate concentrations (Fig. 2A, B). Conversely, the K_d^{ATP} was also dependent on the concentration of cytosolic malate. Reducing cytosolic malate concentrations led to a decreased K_d^{ATP} value (Fig. 2C). The dependency of the inhibition by cytosolic ATP on the concentration of permeable anion suggested a competition mechanism between cytosolic ATP and malate. To extrapolate whether this modulation occurs in the physiological range, a K_d^{ATP} of approximately 50 µM at -160 mV could be determined for malate concentrations in the physiological range (400~ 800 µM) (19-21). These results indicate that the modulation observed by free ATP occurs in the physiological range, since free ATP concentrations deduced from cytosolic ATP and Mg^{2+} concentrations are in the range of 30 to 100 µM (22).

The Anions in the Vacuolar Lumen Affect the Inhibition of *At*ALMT9 by Cytosolic Nucleotides

Recently, we have shown that *At*ALMT9 is also permeable to chloride and that it is involved in chloride accumulation in the vacuole (6). Thus, we tested the effect of free ATP on *At*ALMT9-mediated chloride currents. Similarly to what was observed when malate was the main permeable anion, 1 mM free ATP strongly inhibited *At*ALMT9-mediated chloride currents to 29 ± 3% of the ATP free conditions at -160 mV (100 mM Cl^-_{cyt} + 1mM $malate_{cyt}$ / 100 mM Cl^-_{vac}; Fig. 3). Intriguingly, the I-V curve in chloride conditions inhibited by ATP remained monotonic and did not display a bell-shaped behavior in the investigated voltage range at all tested concentrations of cytosolic ATP (Fig. 3A, left). In these conditions the ATP inhibition started to be effective at membrane potentials more negative than -60 mV (Fig 3B). However, when chloride was the main permeable anion in the cytosolic solution and 100 mM malate was in the vacuolar buffer (100 mM Cl^-_{cyt} + 1mM $malate_{cyt}$ / 100 mM $malate_{vac}$), the inhibitory effect induced by 1 mM free ATP (Fig. 3A, right) resembled that observed in the malate based cytosolic solution (Fig. 1 and 2). Indeed, under these conditions the inhibitory effect of cytosolic ATP starts abruptly at lower membrane potentials (-100 mV). The analysis of the voltage dependency of the ATP blockade shows that the presence of malate instead of Cl^- in the vacuole shifts the effect of cytosolic ATP toward more negative potentials (Fig. 3B). Indeed, the half activation voltage ($V_{1/2}$) was -66 ± 1 mV and -124 ± 1 mV with 100 mM Cl^- or 100 mM malate in the vacuole, respectively (Fig. 3B; Table 1). The maximal inhibition obtained at hyperpolarized voltages t appeared to depend only slightly on the nature of the vacuolar anion, being 24 ± 1% and 31 ± 2% in presence of Cl^- or malate in the vacuole, respectively (Fig. 3B; Table 1).

In order to evaluate whether the presence of malate in the vacuole was affecting the ATP inhibition we progressively raised the vacuolar concentration of malate (0 mM $malate_{vac}$ + 100 mM MES_{vac}, 1 mM $malate_{vac}$

+ 99 mM MES_{vac}, 10 mM $malate_{vac}$ + 90 mM MES_{vac}, 100 mM $malate_{vac}$) while keeping constant the cytosolic solution (100 mM $malate_{cyt}$). The ATP block was shifted toward more negative membrane potentials by vacuolar malate (Fig. 4B). Moreover, in the absence of vacuolar malate the inhibition by 1 mM free ATP did not induce a bell-shaped I-V curve (Fig. 4A) similar to what observed in Cl^- conditions (100 mM Cl^-_{cyt} / 100 mM Cl^-_{vac}). The $V_{1/2}$ was shifted toward more negative values by vacuolar malate (Fig. 4B; Table1). Thus, the permeable anion in the vacuolar buffer affected the inhibitory behavior of cytosolic ATP on *At*ALMT9. This further suggests that cytosolic ATP and malate compete for a binding site that is likely to be located in the conduction pathway of *At*ALMT9 at the cytosolic side.

The Inhibition of *At*ALMT9 by Cytosolic Nucleotides does not Require ATP Hydrolysis

Our data suggest that cytosolic ATP interact with *At*ALMT9 directly blocking the pore. However, in order to definitively exclude the possibility that the effect of ATP was based on a phosphorylation/dephosphorylation mechanism, we used a non-hydrolysable analogue of ATP, AMPPNP. In the presence of 1 mM AMPPNP in the cytosolic solution (100 mM $malate_{cyt}$ + 1 mM ATP or $AMPPNP_{cyt}$ / 100 mM $malate_{vac}$), the amplitudes of AtALMT9 mediated currents at -160 mV were reduced to 26.0 ± 3.0 % (Fig. 5A). AMPPNP showed a similar and even stronger inhibitory effect compared to ATP (Table 1; Fig. 5B). This demonstrates that no phosphorylation of *At*ALMT9 occurs under the experimental setup. We further analyzed the relative importance of the polyphosphate and nucleoside moieties in the block of *At*ALMT9-mediated currents. We found that the progressive reduction of the number of phosphate groups, and thus of negative charges, strongly impacted the inhibitory effect of the nucleotides with ADP being less efficient than ATP (I_{ADP}/I_{ctrl} = 56 ± 2% at -160 mV) and AMP even less (I_{AMP}/I_{ctrl}=90 ± 1% at -160 mV) (Fig. 5A). Differently, the nucleoside part seems to have a marginal role since 1 mM free GTP showed an effect similar to ATP (I_{GTP}/I_{ctrl} = 48 ± 2% at -160 mV; Fig. 5A). These data suggest that the number of charges carried by the nucleotide is fundamental for the block of *At*ALMT9-mediated currents. Cyclic nucleotides such as cAMP and cGMP and the inorganic pyrophosphate (PPi) induced no significant reduction on AtALMT9 mediated currents (Fig 5B). Previously, we found that lysine 193 (K193) is part of the permeation pathway of *At*ALMT9 and its mutation (K193E) affects both anion permeation rectification and the efficiency of citrate to block the currents (7). Thus, in an attempt to find a site of interaction of ATP with the channel, we tested whether the mutation of K193 impacted the ATP blockade. We found that the currents mediated by the $AtALMT9_{K193E}$ variants were completely insensitive to 1 mM free ATP in the cytosolic-side solution (100 mM malate + 1mM ATP_{cyt} / 100 mM $malate_{vac}$; Fig. 5B). These data suggest that cytosolic nucleotides interact with the residue K193 and that the blocking mechanism was similar to the one observed previously for citrate. Therefore, ATP is likely to block *At*ALMT9 mediated currents by obstructing the pore of *At*ALMT9.

DISCUSSION

ALMTs form a family of anion channels playing diverse important functions in plants. Among the different ALMTs, *At*ALMT9 is the first member of the family shown to be localized in the vacuolar membrane (4). *In vivo* *At*ALMT9 acts as a malate activated chloride channel, playing an important role in stomatal opening (6). A further study provided evidence that *At*ALMT9 forms tetramers and the fifth transmembrane α-helix (TMα5) possibly forms the permeation pathway (7). Since the I-V characteristic is a fundamental property of ion channels, in the present work we aimed to find a reason for the different I-V characteristic displayed by different members of the ALMT family. *At*ALMT1 and *At*ALMT9 display a monotonic and moderately voltage dependent inward rectifying I-V characteristics (3,4). Differently, *At*ALMT12/QUAC1 displays an I-V

characteristic with a strong voltage dependency especially at membrane potentials below -100 mV (5). Earlier studies on *Arabidopsis* hypocotyl protoplasts showed that cytosolic ATP regulates the R-type currents (12,13). Thus, a model of the R-type channel which is gated by the cytosolic nucleotides was proposed. The vacuolar localization of *At*ALMT9 appears to be very convenient since it allows the reversible application of nucleotides on the cytosolic side of the membrane, enabling to directly probe the effect of nucleotides on I-V characteristic of *At*ALMT9.

The two main results we present in this work are that cytosolic nucleotides reversibly inhibit *At*ALMT9-mediated currents and that in presence of cytosolic nucleotides the I-V characteristic of *At*ALMT9 changes from monotonic to bell shaped (Fig. 1). In other terms the presence of ATP in the cytosolic solution is sufficient to make *At*ALMT9 display the same bell-shaped I-V characteristic as *At*ALMT12/QUAC1. This intriguing result suggests that the typical bell-shaped I-V characteristic is not a unique property of this clade of the ALMT family and that it does not result from an intrinsic voltage sensor in the ion channel protein. The understanding of the voltage dependency of *At*ALMT9 and *At*ALMT12 is relevant because of their roles in regulating stomatal movement (5,6). Our data indicate that the effect of ATP on *At*ALMT9 currents does not rely on a phosphorylation mechanism but directly by blocking the permeation pathway of the channel. Indeed, the non-hydrolysable ATP analogue AMPPNP is able to block *At*ALMT9 mediated currents. AMPPNP presents a stronger inhibitory effect compared to ATP. This might be due to the presence of a nitrogen atom, forming an imido bond between the β and the γ phosphorus, instead of an oxygen atom forming an anhydride bond. This difference in the phosphoric moiety between the two nucleotides might influence the interaction between the blocker and the channel, consequently affecting the strength of the inhibition. Moreover, several lines of evidence point at an "open-channel block" mechanism. i) The effect is voltage dependent and more pronounced at negative voltages at which the channels' open probability is higher; ii) the dissociation constant (K_d^{ATP}) is voltage dependent, indicating that ATP enters the transmembrane electrical field; iii) the current is more noisy at membrane potentials at which ATP is effective (Fig. 1A); iv) ATP and the permeating anion compete since the K_d^{ATP} becomes lower when malate concentrations decrease (Fig. 2C). It is interesting to note that this is in line with the nucleotide-dependent gating mechanism of the R-type/QUAC channel in the plasma membrane proposed by Colcombet et al. (13). Moreover, our results provide a strong molecular basis to interpret these findings by the identification of K193 as possible interaction site of ATP with *At*ALMT9 (Fig. 5B). Notably, in a previous study we found K193 to be part of a putative pore forming region (7), further supporting the idea that ATP interacts with the pore region of *At*ALMT9.

Since the inhibition of *At*ALMT9 by ATP in malate based solutions transform the I-V curve of this channel from monotonic to bell shaped, similar to the one of R-type channels, our data support the idea that *At*ALMT12/QUAC1 is gated by cytosolic nucleotides and that the typical I-V characteristic of this channel comes from this voltage dependent block. It has to be noted that in all the situations in which *At*ALMT12/QUAC1 has been measured ATP was present in significant amounts in the cytosolic solution (5,8). Moreover, the only attempt to remove ATP from the cytosolic solution revealed a change of the bell-shaped I-V characteristic to monotonic one (13). As a corollary our data also provide a simple and straightforward interpretation of a phenomenon that R-type currents are activated by extracellular malate (23-25). In this work we found that vacuolar malate (which correspond in our configuration to extracellular malate) is able to release the ATP block (Fig. 3 and Fig. 4), consequently inducing an activation of the *At*ALMT9 currents. Thus, the malate activation of *At*ALMT12/QUAC1 would result from a release of ATP block by the presence of extracellular malate.

It is interesting to address the question whether the ATP block of *At*ALMT9 currents can be relevant in a physiological context. Even if presently our data do not directly answer this question we can try to insert them in a physiological framework. The inhibition by ATP starts to be significant at tonoplast membrane potentials between -60 and -80 mV which is probably within the physiological range (Fig 2B; Martinoia et al. 2012). Recently, we have shown that *At*ALMT9 is important in guard cells function for stomatal opening (6). Indeed, during stomatal opening *At*ALMT9 drives the influx of anions into the vacuole. The influx of anion via *At*ALMT9 is driven by hyperpolarized vacuolar membrane potentials which are maintained through H^+-ATPases (26-28). During stomatal opening the high hydrolytic activity of the proton pump consumes ATP, decreasing its concentration in the cytosol. Subsequently, ATP is converted into AMP (29,30) which is nearly inactive in blocking *At*ALMT9 meditated anion currents. Thus, a drop of cytosolic ATP levels could induce a release of the *At*ALMT9 blockage and consequently facilitate anion accumulation in the vacuole. In addition, the accumulation of malate in the vacuolar lumen, which is known to occur in parallel to chloride accumulation, is also able to remove the ATP blockade (Fig. 3, Fig. 4). This blockade release would consequently facilitate anion uptake into the vacuole. Therefore, both cytosolic and vacuolar malate can regulate *At*ALMT9 activity with a direct activation (6) and a release of ATP block, respectively. Since the ATP block efficiency is different in the presence or in the absence of Mg^{2+} (Fig 1H) the regulation of AtALMT9 currents by nucleotides might depend also on fluctuations of the intracellular Mg^{2+} concentration. It is interesting to note that *At*ALMT9 is the second vacuolar anion transporter after *At*CLCa (31) whose activity is inhibited by cytosolic ATP. This further suggests that the regulation of vacuolar anion transporters and channels activity by cytosolic nucleotides has a physiological relevance. Moreover, the modulation of vacuolar anion transporters by cytosolic nucleotides suggests a direct connection between accumulation of anions in the vacuole and the energetic status of the cell.

Considering the data published so far, it is very likely that plasma membrane localized ALMTs exhibit a similar modulation. In this case the modulation of the channel activity by ATP may play an even more important role, since during hyperpolarization events the inhibition of the channel is nearly complete.

REFERENCES

1. Delhaize, E., Ryan, P. R., Hebb, D. M., Yamamoto, Y., Sasaki, T., and Matsumoto, H. (2004) Engineering high-level aluminum tolerance in barley with the ALMT1 gene. *Proc. Natl. Acad. Sci. U S A* **101**, 15249-15254
2. Sasaki, T., Yamamoto, Y., Ezaki, B., Katsuhara, M., Ahn, S. J., Ryan, P. R., Delhaize, E., and Matsumoto, H. (2004) A wheat gene encoding an aluminum-activated malate transporter. *Plant J.* **37**, 645-653
3. Hoekenga, O. A., Maron, L. G., Pineros, M. A., Cancado, G. M. A., Shaff, J., Kobayashi, Y., Ryan, P. R., Dong, B., Delhaize, E., Sasaki, T., Matsumoto, H., Yamamoto, Y., Koyama, H., and Kochian, L. V. (2006) AtALMT1, which encodes a malate transporter, is identified as one of several genes critical for aluminum tolerance in Arabidopsis. *Proc. Natl. Acad. Sci. USA* **103**, 9738-9743
4. Kovermann, P., Meyer, S., Hortensteiner, S., Picco, C., Scholz-Starke, J., Ravera, S., Lee, Y., and Martinoia, E. (2007) The Arabidopsis vacuolar malate channel is a member of the ALMT family. *Plant J.* **52**, 1169-1180
5. Meyer, S., Mumm, P., Imes, D., Endler, A., Weder, B., Al-Rasheid, K. A. S., Geiger, D., Marten, I., Martinoia, E., and Hedrich, R. (2010) AtALMT12 represents an R-type anion channel required for stomatal movement in Arabidopsis guard cells. *Plant J.* **63**, 1054-1062
6. De Angeli, A., Zhang, J., Meyer, S., and Martinoia, E. (2013) AtALMT9 is a malate-activated vacuolar chloride channel required for stomatal opening in Arabidopsis. *Nat. commun.* **4**, 1804
7. Zhang, J., Baetz, U., Krugel, U., Martinoia, E., and De Angeli, A. (2013) Identification of a probable pore forming domain in the multimeric vacuolar anion channel AtALMT9. *Plant Physiol.* **163**, 830-843
8. Sasaki, T., Mori, I. C., Furuichi, T., Munemasa, S., Toyooka, K., Matsuoka, K., Murata, Y., and Yamamoto, Y. (2010) Closing plant stomata requires a homolog of an aluminum-activated malate transporter. *Plant Cell Physiol.* **51**, 354-365
9. Meyer, S., Scholz-Starke, J., De Angeli, A., Kovermann, P., Burla, B., Gambale, F., and Martinoia, E. (2011) Malate transport by the vacuolar AtALMT6 channel in guard cells is subject to multiple regulation. *Plant J.* **67**, 247-257
10. Hedrich, R., Busch, H., and Raschke, K. (1990) Ca2+ and nucleotide dependent regulation of voltage dependent anion channels in the plasma membrane of guard cells. *EMBO J.* **9**, 3889-3892
11. SchulzLessdorf, B., Lohse, G., and Hedrich, R. (1996) GCAC1 recognizes the pH gradient across the plasma membrane: A pH-sensitive and ATP-dependent anion channel links guard cell membrane potential to acid and energy metabolism. *Plant J.* **10**, 993-1004
12. Thomine, S., Guern, J., and Barbier-Brygoo, H. (1997) Voltage-Dependent Anion Channel of Arabidopsis Hypocotyls: Nucleotide Regulation and Pharmacological Properties. *J. Membrane Biol.* **159**, 71-82
13. Colcombet, J., Thomine, S., Guern, J., Frachisse, J. M., and Barbier-Brygoo, H. (2001) Nucleotides provide a voltage-sensitive gate for the rapid anion channel of arabidopsis hypocotyl cells. *J. Biol. Chem.* **276**, 36139-36145
14. Lopatin, A. N., Makhina, E. N., and Nichols, C. G. (1994) Potassium Channel Block by Cytoplasmic Polyamines as the Mechanism of Intrinsic Rectification. *Nature* **372**, 366-369
15. Lu, Z. (2004) Mechanism of rectification in inward-rectifier K+ channels. *Annu. Rev. Physiol.* **66**, 103-129
16. Yang, K. Y., Liu, Y. D., and Zhang, S. Q. (2001) Activation of a mitogen-activated protein kinase pathway is involved in disease resistance in tobacco. *Proc. Natl. Acad. Sci. USA* **98**, 741-746

17. Neher, E. (1992) Correction for liquid junction potentials in patch clamp experiments. *Methods Enzymol* **207**, 123-131
18. Woodhull, A. M. (1973) Ionic blockage of sodium channels in nerve. *J. Gen. Physiol.* **61**, 687-708
19. Gerhardt, R., and Heldt, H. W. (1984) Measurement of Subcellular Metabolite Levels in Leaves by Fractionation of Freeze-Stopped Material in Nonaqueous Media. *Plant Physiol.* **75**, 542-547
20. Winter, H., Robinson, D. G., and Heldt, H. W. (1994) Subcellular Volumes and Metabolite Concentrations in Spinach Leaves. *Planta* **193**, 530-535
21. Farre, E. M., Tiessen, A., Roessner, U., Geigenberger, P., Trethewey, R. N., and Willmitzer, L. (2001) Analysis of the compartmentation of glycolytic intermediates, nucleotides, sugars, organic acids, amino acids, and sugar alcohols in potato tubers using a nonaqueous fractionation method. *Plant Physiol.* **127**, 685-700
22. Yazaki, Y., Asukagawa, N., Ishikawa, Y., Ohta, E., and Sakata, M. (1988) Estimation of Cytoplasmic Free Mg2+ Levels and Phosphorylation Potentials in Mung Bean Root Tips by In Vivo 31P NMR Spectroscopy. *Plant Cell Physiol.* **29**, 919-924
23. Hedrich, R., and Marten, I. (1993) Malate-Induced Feedback-Regulation of Plasma-Membrane Anion Channels Could Provide a Co2 Sensor to Guard-Cells. *EMBO J.* **12**, 897-901
24. Raschke, K. (2003) Alternation of the slow with the quick anion conductance in whole guard cells effected by external malate. *Planta* **217**, 651-657
25. Mumm, P., Imes, D., Martinoia, E., Al-Rasheid, K. A., Geiger, D., Marten, I., and Hedrich, R. (2013) C-terminus mediated voltage gating of Arabidopsis guard cell anion channel QUAC1. *Mol. Plant* **6**, 1550-1563
26. Gaxiola, R. A., Palmgren, M. G., and Schumacher, K. (2007) Plant proton pumps. *FEBS Lett.* **581**, 2204-2214
27. Duby, G., and Boutry, M. (2009) The plant plasma membrane proton pump ATPase: a highly regulated P-type ATPase with multiple physiological roles. *Pflug Arch Eur J Phy* **457**, 645-655
28. Palmgren, M. G., and Nissen, P. (2011) P-Type ATPases. *Annu. Rev. Biophys., Vol 40* **40**, 243-266
29. Gout, E., Bligny, R., and Douce, R. (1992) Regulation of intracellular pH values in higher plant cells. Carbon-13 and phosphorus-31 nuclear magnetic resonance studies. *J. Biol. Chem.* **267**, 13903-13909
30. Xia, J. H., Saglio, P., and Roberts, J. K. M. (1995) Nucleotide Levels Do Not Critically Determine Survival of Maize Root-Tips Acclimated to a Low-Oxygen Environment. *Plant Physiol.* **108**, 589-595
31. De Angeli, A., Moran, O., Wege, S., Filleur, S., Ephritikhine, G., Thomine, S., Barbier-Brygoo, H., and Gambale, F. (2009) ATP Binding to the C Terminus of the Arabidopsis thaliana Nitrate/Proton Antiporter, AtCLCa, Regulates Nitrate Transport into Plant Vacuoles. *J. Biol. Chem.* **284**, 26526-26532

Footnotes

This work was supported by the Chinese Scholarship Council (to J.Z.) and by the Swiss National Foundation (to E.M. and A.D.A).

FIGURE LEGENDS

Figure 1. Cytosolic ATP reversibly blocks *At*ALMT9 mediated currents in a voltage dependent fashion.

(A, B,C) Representative traces and corresponding I-V curves of excised cytosolic-side out patches from *N. benthamiana* vacuoles overexpressing *At*ALMT9 in 30 mM $malate_{cyt}$ / 100 mM $malate_{vac}$. (A), 30 mM $malate_{cyt}$ + 1 mM ATP_{free} / 100 mM $malate_{vac}$ (B), recovery (C). Currents were evoked in response to 3 s voltage pulses ranging from +60 mV to -160 mV in -20 mV steps, followed by a tail pulse at +60 mV. The holding potential was set at +60 mV. Red highlights the currents at the membrane potentials where the ATP inhibition is effective. (D) Ratio between currents measured in the absence (I_{ctrl}, 30 mM $malate_{cyt}$ / 100 mM $malate_{vac}$) and in the presence of the indicated concentrations of ATP_{cyt} (I_{ATP}, 30 mM $malate_{cyt}$ + X mM ATP_{free}/ 100 mM $malate_{vac}$) at different applied membrane potentials. Data were fitted with equation 3 (see Materials and Methods; dashed line) (n= 4~7). (E) Dose response curves for ATP_{free} at different membrane potentials. Data were fitted with equation 1 (see Materials and Methods; solid lines) to derive the dissociation constant (K_d^{ATP}). (F) Voltage dependency of the dissociation constant for ATP (K_d^{ATP}) in 30 mM $malate_{cyt}$ / 100 mM $malate_{vac}$. Solid line, data were fitted with equation 2. (G, H) Inhibitory effect of Mg-ATP. (G) Normalized current-voltage curves were obtained with a voltage ramp (from +60 mV to -160 mV in 1.5s) with 30 mM $malate_{cyt}$ / 100 mM $malate_{vac}$ and in 30 mM $malate_{cyt}$ / 100 mM $malate_{vac}$ in the presence of 1 mM ATP_{free} (+ 1 mM ATP) or Mg-ATP (1 mM Mg-ATP). (H), residual currents (I_{ATP}/I_{ctrl}; mean ± SEM, n=3-7) plotted against the applied voltage in presence of 1 mM ATP_{free} or Mg-ATP. Data were fitted with equation 3 (dashed line). Error bars denote s.e.m.-

Figure 2. Cytosolic ATP compete with cytosolic malate to inhibit *At*ALMT9-mediated currents

(A) Normalized current-voltage curves obtained with a voltage ramp protocol (from +60 mV to -160 mV in 1.5 s) in cytosolic-side buffers containing various concentrations of malate (30 mM, 50 mM and 100 mM $malate_{cyt}$) with constant vacuolar side conditions(100 mM $malate_{vac}$) in the presence (+ATP) or absence of 1 mM ATP_{free}. (B) Fraction of unblocked current in presence of 1 mM ATP_{free} (I_{ATP}/I_{ctrl} ; mean ± SEM, n=4-7) plotted against the applied voltage in different cytosolic malate concentrations. Data were fitted with equation 3 (Materials and Methods; Table 1; solid line). (C) logarithmic plot of the dissociation constant for ATP_{free} (K_d^{ATP}) at different applied membrane potentials (-120 mV, -140 mV and -160 mV) shown as a function of different cytosolic malate concentrations (30, 50, 100 mM $malate_{cyt}$). Data were fitted with a straight line with no theoretical significance to extrapolate the value of the dissociation constant at malate concentrations in the physiological range. Error bars denote s.e.m.

Figure 3 Vacuolar anions affect the ATP-dependent block of *At*ALMT9 mediated chloride currents

(A) Normalized AtLMT9 mediated currents elicited by a voltage ramp from +60 mV to -160 mV in 1.5 s (holding potential +60 mV) with a chloride based cytosolic buffer in presence (+ATP) or absence of 1 mM ATP_{free}. The vacuolar buffers contained 100 mM Cl^- (*left panel*;

100 mM Cl^- + 1 mM $malate_{cyt}$ / 100 mM Cl^-_{vac}) or malate (*right panel*;100 mM Cl^- + 1 mM $malate_{cyt}$ / 100 mM $malate_{vac}$). (B) Fraction of unblocked current (I_{ATP}/I_{ctrl} ; mean ± SEM, n=4) plotted against the applied membrane potential in presence of 100 mM Cl^- or 100 mM malate in the vacuolar buffer. Data were fitted with equation 3 (Materials and methods; Table 1; dashed lines) yielding $V_{1/2}$ = -66 ± 1 mV (100 mM Cl^-_{vac}) and $V_{1/2}$ = -124 ± 1 mV (100 mM $malate_{vac}$). Error bars denote s.e.m.

Figure 4. Vacuolar malate relieves cytosolic ATP inhibition.

(A) Currents elicited by a voltage ramp from +60 mV to -160 mV in 1.5 s (holding potential +60 mV) in presence of a cytosolic-side buffer containing 100 mM malate and vacuolar-side buffers containing 0 mM malate (100 mM $malate_{cyt}$ / 100 mM MES_{vac}), 1 mM malate (100 mM $malate_{cyt}$ / 1 mM malate + 99 mM MES_{vac}), 10 mM malate (100 mM $malate_{cyt}$ / 10 mM malate + 90 mM MES_{vac}), 100 mM malate (100 mM $malate_{cyt}$ / 100 mM $malate_{vac}$), in the absence or the presence of 1 mM ATP_{free} (+ATP) in cytosolic-side buffer. (B) Ratios ($I_{ATP}/I_{Ctrl,}$ mean ± SEM, n=5-7) between currents recorded in presence (I_{ATP}) and the absence (I_{ctrl}) of 1 mM ATP_{free} with the progressive increase of vacuolar malate concentration as indicated (cytosolic buffer was kept constant with 100 mM malate). The solid lines represent data fit with equation 3 (Materials and Methods; Table 1). Error bars denote s.e.m.

Figure 5. Effect of the non-hydrolysable nucleotide AMPPNP and of different cytosolic nucleotides on *At*ALMT9 mediated malate currents.

(A*)* Left panel: Representative currents elicited by a voltage ramp (from +60 mV to -160 mV in 1.5 s, holding potential +60 mV) in 100 mM $malate_{cyt}$ /100 mM $malate_{vac}$ (ctrl) and in 100 mM $malate_{cyt}$ /100 mM $malate_{vac}$ + 1 mM of different nucleotides in the cytosolic-side buffer: ATP, ADP, AMP, GTP. Right panel: mean current ratios between currents in presence of 1 mM the indicated nucleotide (I_n) and control conditions (I_{ctrl}) at different membrane potentials (n= 4-7). (B) Left panel :I-V curves elicited as in (A) in 100 mM $malate_{cyt}$ and 100 mM $malate_{vac}$ (ctrl) and in 100 mM $malate_{cyt}$ and 100 mM $malate_{vac}$ in the presence of 1mM cAMP, cGMP, PPi and AMPPNP. Right panel: mean current ratios between currents in presence of 1 mM of the indicated nucleotide (I_n) and control conditions (I_{ctrl}) at different membrane potentials of cAMP, cGMP, PPi and AMPPNP and currents measured in, (n=3-4). (C) left panel: representative currents obtained as in (A) in excised cytosolic-side out patches from vacuoles overexpressing $AtALMT9_{WT}$ and $AtALMT9_{K193E}$ (n=6) in the presence (+ATP) or absence of 1 mM ATP_{free} (100 mM $malate_{cyt}$ / 100 mM $malate_{vac}$). Right panel: mean current ratios of $AtALMT9_{WT}$ and $AtALMT9_{K193E}$ currents in presence (I_{ATP}) or absence (I_{ctrl}) of 1 mM ATP_{free} at different membrane potentials. Dashed lines indicate the tendency but have no theoretical meaning. Error bars denote s.e.m.

Ionic Conditions			I_{ATP}/I_0 at -160 mV(%)	Parameters		
Cytosolic	Vacuolar	ATP_{cyt}/mM		$V_{1/2}$/mV	I_{unh}(%)	Location
30 mM malate	100 mM malate	0.1	46 ± 1	-131 ± 4	40 ± 7	Fig. 1B
30 mM malate	100 mM malate	0.5	17 ± 1	-118 ± 1	16 ± 3	Fig. 1B
30 mM malate	100 mM malate	1	10 ± 1	-114 ± 0.8	6 ± 2	Fig. 1B
50 mM malate	100 mM malate	1	19 ± 2	-119 ± 4	11 ± 5	Fig. 2B
100 mM malate	100 mM malate	1	37 ± 2	-135 ± 2	32 ± 5	Fig. 2B
100 mM Cl^-	100 mM Cl^-	1	29 ± 3	- 66 ± 1	24 ± 1	Fig. 3B
100 mM Cl^-	100 mM malate	1	34 ± 2	-124 ± 1	31 ± 2	Fig. 3B
100 mM malate	0 mM malate	1	44 ± 2	-112 ± 4	38 ± 4	Fig. 4B
100 mM malate	1 mM malate	1	42 ± 1	- 113 ± 2	39 ± 3	Fig. 4B
100 mM malate	10 mM malate	1	38 ± 3	- 119 ± 3	31 ± 4	Fig. 4B
100 mM malate	100 mM Cl^-	1	41 ± 3	- 135 ± 13	7 ± 16	Fig. 4B

Table1. Parameters of the Boltzmann fits (equation 3) in different experimental conditions. I_{ATP}/I_0 is the ratio between the current measured in presence of ATP and in cytosolic solutions without ATP. I_{unh} the residual current in presence of ATP, $V_{1/2}$ is the potential at which half of the current was blocked. . Data are presented as means ± SD

FIGURE 1

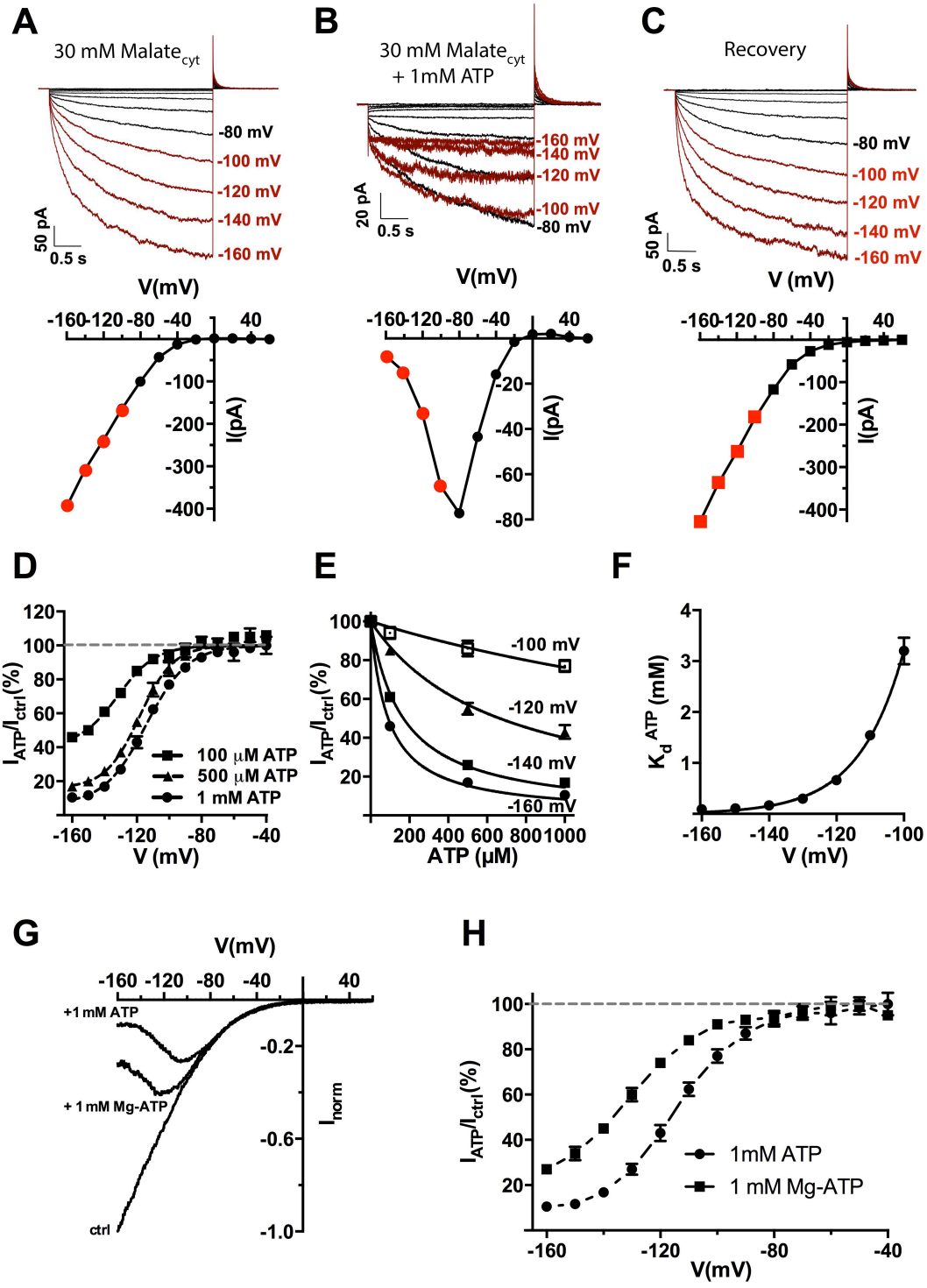
A
30 mM Malate$_{cyt}$
-80 mV
-100 mV
-120 mV
-140 mV
-160 mV
50 pA
0.5 s
V(mV)
-160 -120 -80 -40 40
-100
-200
-300
-400
I(pA)
B
30 mM Malate$_{cyt}$
+ 1mM ATP
-160 mV
-140 mV
-120 mV
-100 mV
-80 mV
20 pA
0.5 s
V(mV)
-160 -120 -80 -40 40
-20
-40
-60
-80
I(pA)
C
Recovery
-80 mV
-100 mV
-120 mV
-140 mV
-160 mV
50 pA
0.5 s
V (mV)
-160 -120 -80 -40 40
-100
-200
-300
-400
I(pA)
D
120
100
80
60
40
20
I_{ATP}/I_{ctrl}(%)
100 µM ATP
500 µM ATP
1 mM ATP
-160 -120 -80 -40
V (mV)
E
100
80
60
40
20
I_{ATP}/I_{ctrl}(%)
-100 mV
-120 mV
-140 mV
-160 mV
200 400 600 800 1000
ATP (µM)
F
4
3
2
1
K_d^{ATP} (mM)
-160 -140 -120 -100
V (mV)
G
V(mV)
-160 -120 -80 -40 40
+1 mM ATP
+ 1 mM Mg-ATP
ctrl
-0.2
-0.6
-1.0
I_{norm}
H
100
80
60
40
20
I_{ATP}/I_{ctrl}(%)
1mM ATP
1 mM Mg-ATP
-160 -120 -80 -40
V(mV)

FIGURE 2

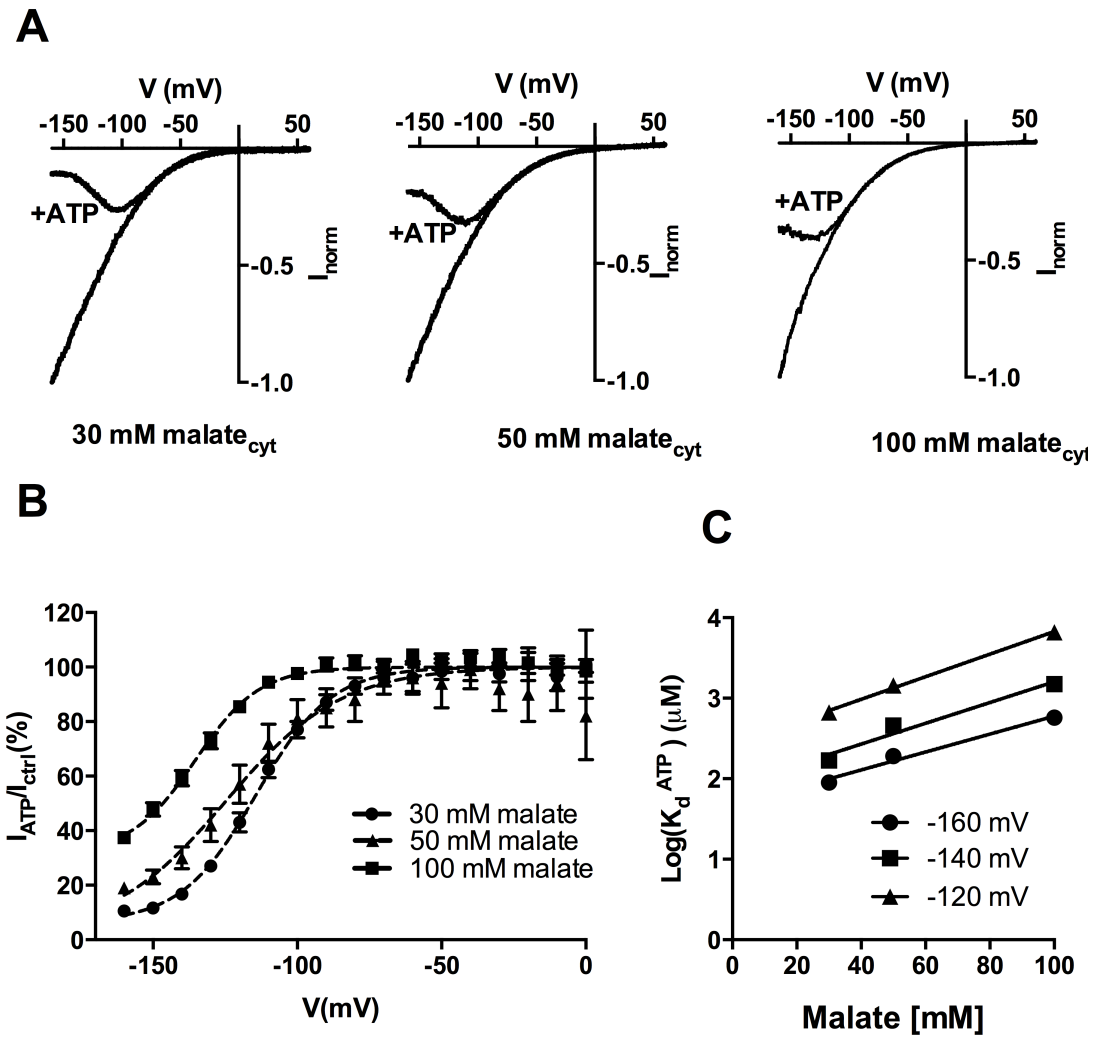
A
V (mV)
-150 -100 -50 50
+ATP
-0.5
-1.0
I norm
30 mM malate cyt
50 mM malate cyt
100 mM malate cyt
B
I ATP/I ctrl (%)
120
100
80
60
40
20
0
-150 -100 -50 0
V(mV)
30 mM malate
50 mM malate
100 mM malate
C
Log(K d ATP) (µM)
4
3
2
1
0
0 20 40 60 80 100
Malate [mM]
-160 mV
-140 mV
-120 mV

FIGURE 3

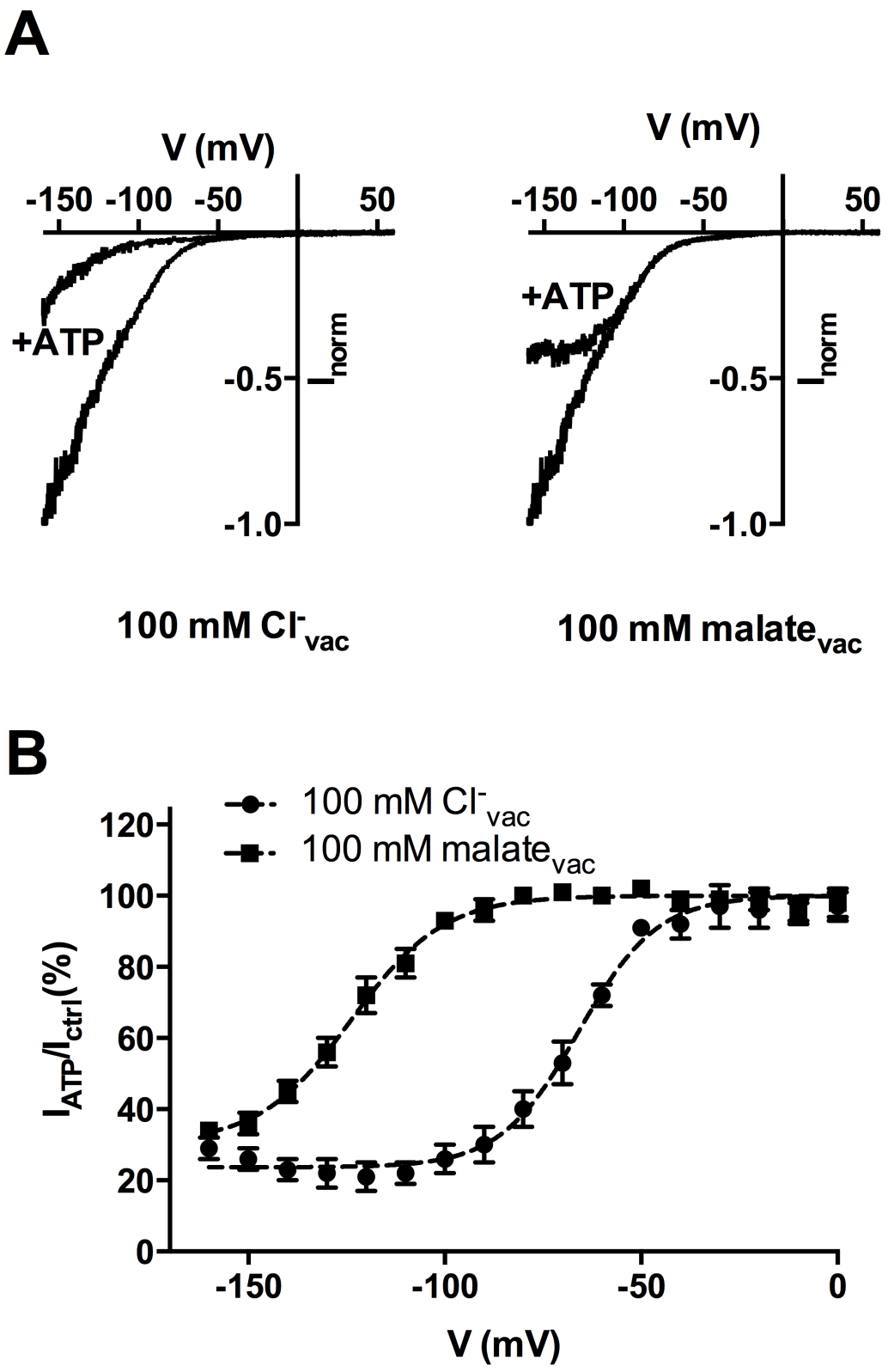
A
V (mV)
-150 -100 -50 50
+ATP
-0.5
-1.0
I_{norm}
100 mM Cl^-_{vac}
V (mV)
-150 -100 -50 50
+ATP
-0.5
-1.0
I_{norm}
100 mM $malate_{vac}$
B
100 mM Cl^-_{vac}
100 mM $malate_{vac}$
I_{ATP}/I_{ctrl}(%)
120
100
80
60
40
20
0
-150
-100
-50
0
V (mV)

FIGURE 4

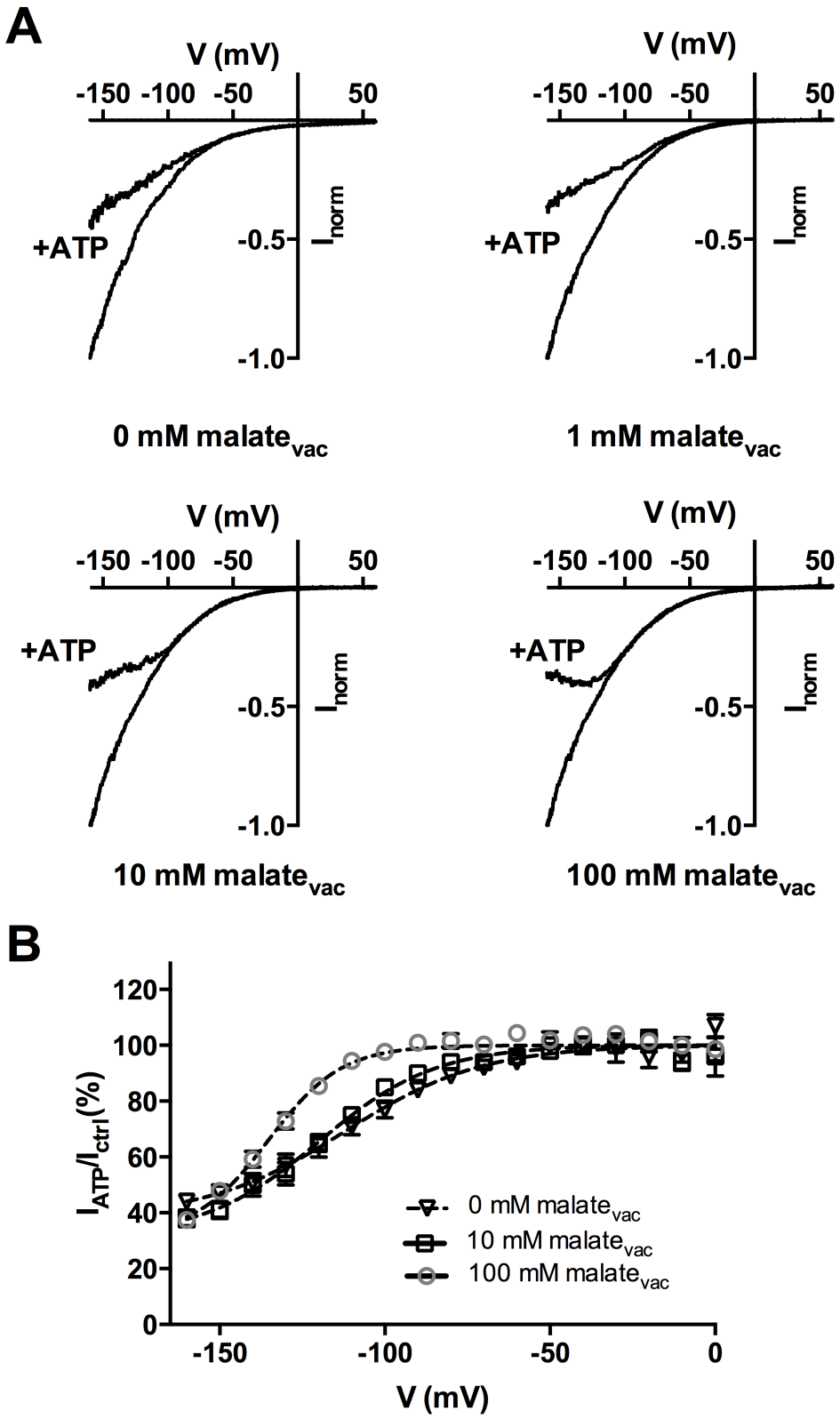
A
V (mV)
-150 -100 -50 50
+ATP
-0.5
-1.0
I norm
0 mM malate vac
1 mM malate vac
10 mM malate vac
100 mM malate vac
B
I ATP/I ctrl (%)
120
100
80
60
40
20
0
-150 -100 -50 0
V (mV)
0 mM malate vac
10 mM malate vac
100 mM malate vac

FIGURE 5

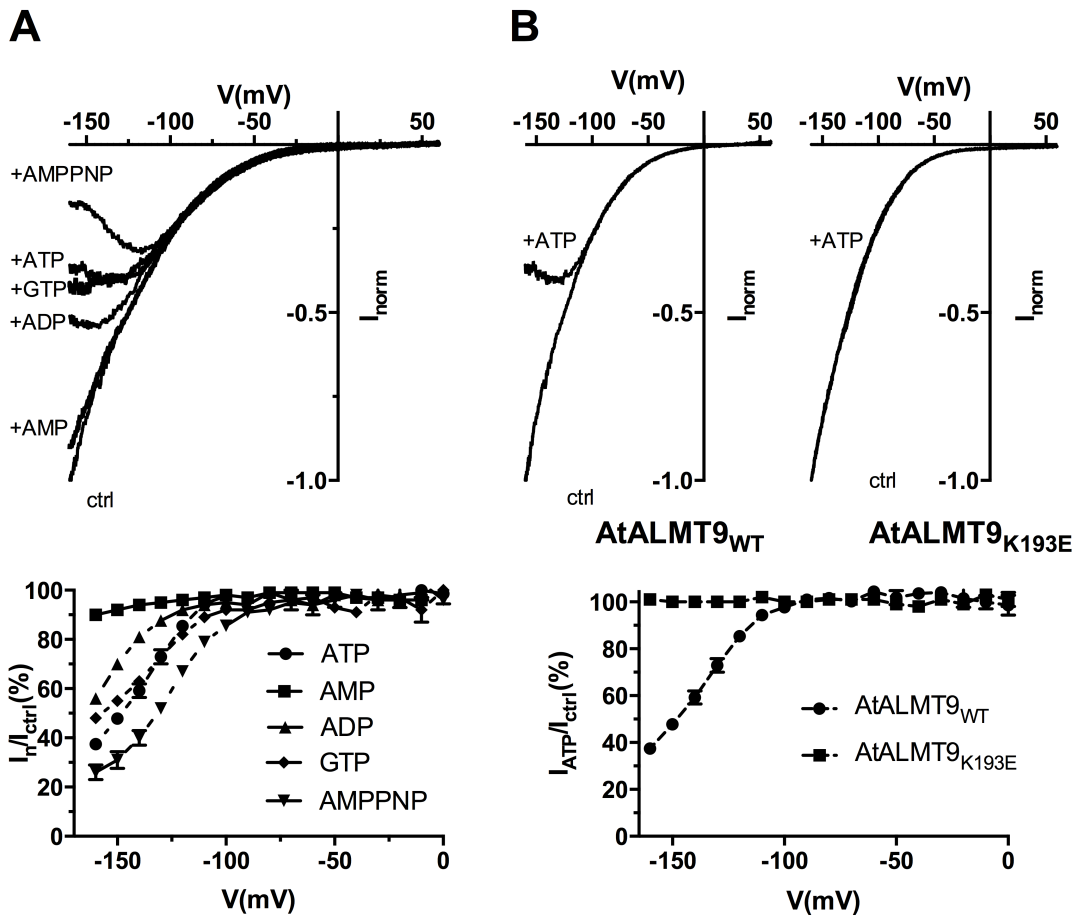
A
B
V(mV)
-150
-100
-50
50
+AMPPNP
+ATP
+GTP
+ADP
+AMP
ctrl
-0.5
-1.0
I_{norm}
$AtALMT9_{WT}$
$AtALMT9_{K193E}$
I_n/I_{ctrl}(%)
ATP
AMP
ADP
GTP
AMPPNP
I_{ATP}/I_{ctrl}(%)
$AtALMT9_{WT}$
$AtALMT9_{K193E}$
0
20
40
60
80
100